This is the accepted manuscript made available via CHORUS. The article has been published as:

Low-energy magneto-optics of math xmlns="http://www.w3.org/1998/Math/MathML">mrow>msub>mi>Tb/mi>mn>2/mn>/msub>msub>mi>Ti/mi>mn>2/mn>/msub>msub>mi mathvariant="normal">O/mi>mn>7/mn>/msub>/mrow>/math> in a [111] magnetic field

Xinshu Zhang, Yi Luo, T. Halloran, J. Gaudet, Huiyuan Man, S. M. Koohpayeh, and N. P. Armitage

Phys. Rev. B **103**, L140403 — Published 12 April 2021

DOI: 10.1103/PhysRevB.103.L140403

Low Energy Magneto-optics of $Tb_2Ti_2O_7$ in [111] Magnetic Field

Xinshu Zhang,[1] Yi Luo,[1] T. Halloran,[1] J. Gaudet,[1] Huiyuan Man,[1] S. M. Koohpayeh,[1,2] and N. P. Armitage[1]

[1]*Institute for Quantum Matter, Department of Physics and Astronomy, The Johns Hopkins University, Baltimore, Maryland 21218, USA*

[2]*Department of Materials Science and Engineering, The Johns Hopkins University, Baltimore, Maryland 21218, USA*

(Dated: March 29, 2021)

The pyrochlore magnet $Tb_2Ti_2O_7$ shows a lack of magnetic order to low temperatures and is considered to be a quantum spin liquid candidate. We perform time-domain THz spectroscopy on high quality $Tb_2Ti_2O_7$ crystal and study the low energy excitations as a function of [111] magnetic field with high energy resolution. The low energy crystal field excitations change their energies anomalously under magnetic field. Despite several sharp field dependent changes, we show that the material's spectrum can be described not by a phase transitions, but by field dependent hybridization between the low energy crystal field levels. We highlight the strong coupling between spin and lattice degrees of freedom in $Tb_2Ti_2O_7$ as evidenced by the magnetic field tunable crystal field environment. Calculations based on single ion physics with field induced symmetry reduction of the crystal field environment can reproduce our data.

Geometric frustration is a central theme in quantum magnets as it suppresses long range magnetic order and frequently causes interesting low temperature states [1]. Rare earth pyrochlores with corner sharing tetrahedra of magnetic ions have strong geometric frustrations. They have been subjects of intense interest for many years [2, 3]. Famous examples include canonical spin ice compound $Dy_2Ti_2O_7$ and $Ho_2Ti_2O_7$, where at low temperature spins follow a two-in-two-out "ice rule" on the tetrahedra and the low energy magnetic excitations are magnetic monopoles connected by a Dirac string [4–7]. Quantum spin liquids (QSLs) are states where spins do not order down to zero temperature and remain dynamic [8, 9]. They have attracted attention for decades due to the potential for exotic quasiparticles as well as potential applications to quantum computation [10–13]. $Yb_2Ti_2O_7$ was once deemed to be quantum spin ice (QSI), but recently experiments on high quality single crystals suggest a coexistence and competition of ferro and anti-ferromagnetism [14–19]. It is believed that $Tb_2Ti_2O_7$ may be a QSL [20]. Unlike $Yb_2Ti_2O_7$ that orders at 270 mK, $Tb_2Ti_2O_7$ shows no magnetic order down to 50 mK despite an anti-ferromagnetic Curie-Weiss temperature $\theta_{CW} \approx 19$ K [21, 22]. Neutron scattering shows power law correlations [23], that bear resemblance to the pinch points found in classical spin ice. μSR shows persistent spin fluctuations down to 70 mK with a relaxation rate 0.04 THz, supporting spin liquid behavior [20].

$Tb_2Ti_2O_7$ is unique among the pyrochlore titanate family for having particularly low energy crystal electric field levels (CEF) and a strong spin-lattice coupling, which are believed to be important for the spin liquid physics. The trigonal symmetry CEF acting on the Tb^{3+} ion leads to a low energy first excited doublet that is separated from the ground state doublet by $\Delta \sim 0.4$ THz (1.6 meV) [22, 24–27]. This is in contrast to other pyrochlore titanates, where the lowest excited CEF level is well isolated from the ground state [22]. Virtual crystal field excitation scenarios and upper branch magnetism have been proposed for $Tb_2Ti_2O_7$ to account for spin liquid physics [28, 29]. Moreover, because Tb^{3+} is a non-Kramers ion, $Tb_2Ti_2O_7$ is susceptible to distortions. Although the presence of static distortions have been debated [30–33], many experiments have demonstrated the strong coupling between spin and lattice degrees of freedom. For instance, giant magnetostriction [34], a coupling between CEF levels and a transverse phonon [35–37], dynamic structural fluctuations as well as a structural transition in pulsed magnetic field have been reported in $Tb_2Ti_2O_7$ [38, 39], suggesting the important role of the lattice. Recently, Raman scattering measurements have reported anomalous CEF excitations with [111] magnetic field, which have been interpreted as a structural phase transition $\sim$2.5 T, leading to electric dipoles induced by magnetic monopoles [40].

In this work, we perform time-domain THz spectroscopy (TDTS) on high quality single crystal $Tb_2Ti_2O_7$ to study the evolution of the low energy crystal field excitations as function of magnetic field along [111] direction. We observed several crystal field anomalies. Although the sharpness of these anomalies might have been taken to be evidence for a field dependent phase transition, we show that such an interpretation is not necessary. Field dependent changes to the CEF environment can capture the essential features of the experiment.

TDTS measurements were performed on optically clear traveling solvent floating zone grown crystals in a custom-built polarization modulation set-up with a frequency range from 0.2 to 2 THz (0.83-8.3 meV) [41] that all components of the transmission tensor (T_{xx}, T_{xy}) can be measured. In contrast to the interferometer used in [42], TDTS is a phase sensitive technique, which allows us to measure the complex THz transmission of a $3\times3\times0.15$ mm^3 single crystal down to 1.6 K with exter-

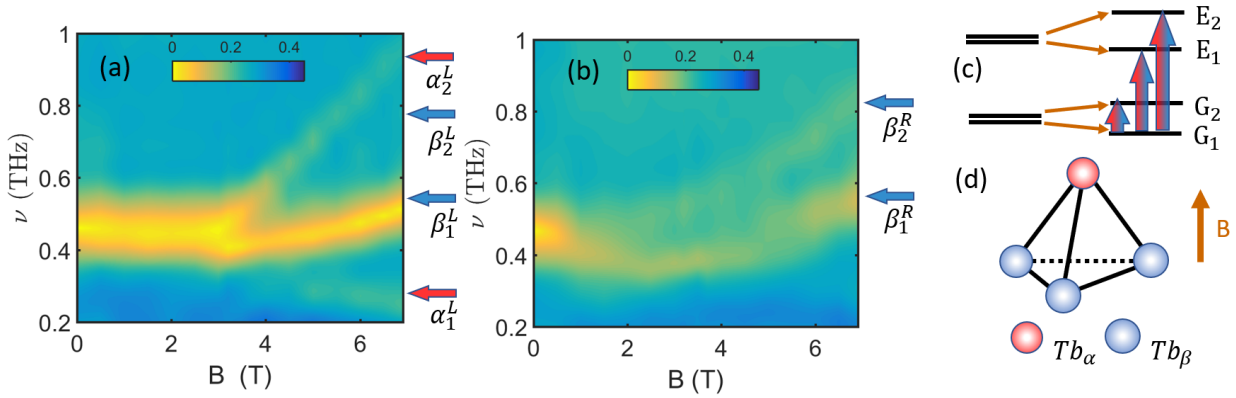


FIG. 1. Transmission amplitude for **(a)** left and **(b)** right circularly polarized THz light as a function of frequency and magnetic field up to 6.9 T at 1.6 K. Four excitations are observed in left channel indicated by α_1^L, β_1^L,β_2^L, α_2^L and two excitations in right channel indicated by β_1^R and β_2^R. **(c)** schematic of CEF splitting in magnetic field labelled as G_1, G_2, E_1 and E_2. The red and blue arrows indicate transitions at two different sites α and β. **(d)** Tetrahedron with red and blue spheres represent the two different Tb ions under [111] magnetic field.

nal fields up to 6.9 T in the Faraday ($\mathbf{k} \parallel \mathbf{H_{dc}}$) geometry, where $\mathbf{k}$ is the direction of light propagation. Under magnetic field, the linearly polarized THz pulse rotates and becomes elliptically polarized as it passes through the sample due to the Faraday rotation. The complex transmission in the Faraday geometry in the linear basis can be converted to the circular basis via the expression $T_{R,L} = T_{xx} \pm iT_{xy}$ [43, 44]. The circular basis are eigenpolarization for transmission in a cubic lattice under magnetic field [45, 46]. The THz transmission in a thick single crystal is a measure of the complex susceptibility [43, 47]. Fig. 1(a) and (b) show transmission magnitudes as a function of frequency and magnetic field at a temperature of 1.6 K for left and right circularly polarized light THz light. A number of excitations are seen as bright yellow features, which correspond to CEF excitations. The fact that different excitations are observed in the two channels correspond to their distinct selection rules.

The observed excitations are expected to originate from transitions from the ground state doublet (G_1 and G_2) to the first excited state doublet (E_1 and E_2), as higher excited states are at much larger energies [24–27]. In zero magnetic field, in the basis of $|m\rangle$=$|J$=6; J_z=$m\rangle$ the ground state doublet is approximately $\psi_{G_{1,2}} \approx a_G|\pm 4\rangle \pm b_G|\mp 5\rangle$ and the first excited state is approximately $\psi_{E_{1,2}} \approx a_E|\pm 5\rangle \pm b_E|\mp 4\rangle$. Applying magnetic field along [111], the ground and first excited state doublets split. Because the experiments were performed at 1.6 K ($\approx$ 0.03 THz and 0.13 meV) the thermal population of all higher levels in high field are negligible and hence only the transitions starting from the ground state G_1 are important. There are two distinct Tb sites (α and β) differentiated by their alignment to the [111] field as shown in Fig. 1(d). Hence, there are 6 different transitions expected, but in experiment not all of them can be seen due to optical selection rules, experimental resolution and limited THz range, etc. We observe four features in the left channel Fig. 1(a) (α_1^L, β_1^L, β_2^L, α_2^L) and two in the right channel Fig. 1(b) (β_1^R, β_2^R). As discussed below, features β_1^L/ β_1^R and β_2^L/β_2^R correspond to the same transitions, which appears in both channels. α_1^L and α_2^L only appear in the L channel due to selection rules. Other notable aspects of the data include an almost constant CEF excitation α_2^L up to 3 T, which then changes its behavior abruptly near 3 T, a behavior that is in stark contrast to the common Zeeman splitting, and a seemingly "new" excitation α_1^L that shows increasing intensity with magnetic field.

To gain further insight on this data, we performed calculations based on single ion physics for D_{3d} point symmetry for Tb^{3+}. The effective Hamiltonian in terms of Stevens operators O_k^q, which applies for a basis comprised of a single J level (J=6 for Tb^{3+}) in the LS coupling scheme, is

$$H_{CEF} = \theta_2 D_2^0 O_2^0 + \theta_4 D_4^0 O_4^0 + \theta_4 D_4^3 O_4^3 + \theta_6 D_6^0 O_6^0 + \theta_6 D_6^3 O_6^3 + \theta_6 D_6^6 O_6^6, \quad (1)$$

where θ_k are the reduced matrix elements. Crystal field parameters B_q^k are obtained by fitting to zero field neutron crystal field energies with the k averaged lowest excitation at 1.6 meV replaced by ~1.9 meV at the Γ point as observed in THz spectroscopy [24]. D_k^q and B_q^k are related by $D_k^q = \lambda_k^q B_q^k$ [48]. The obtained B_q^k parameters are given in the Supplementary Material (SM) [49] and are close to previous works [24]. θ_k and λ_k^q values are also given in the SM [49].

In order to account for the evolution of crystal field excitations as function of magnetic field, we include a

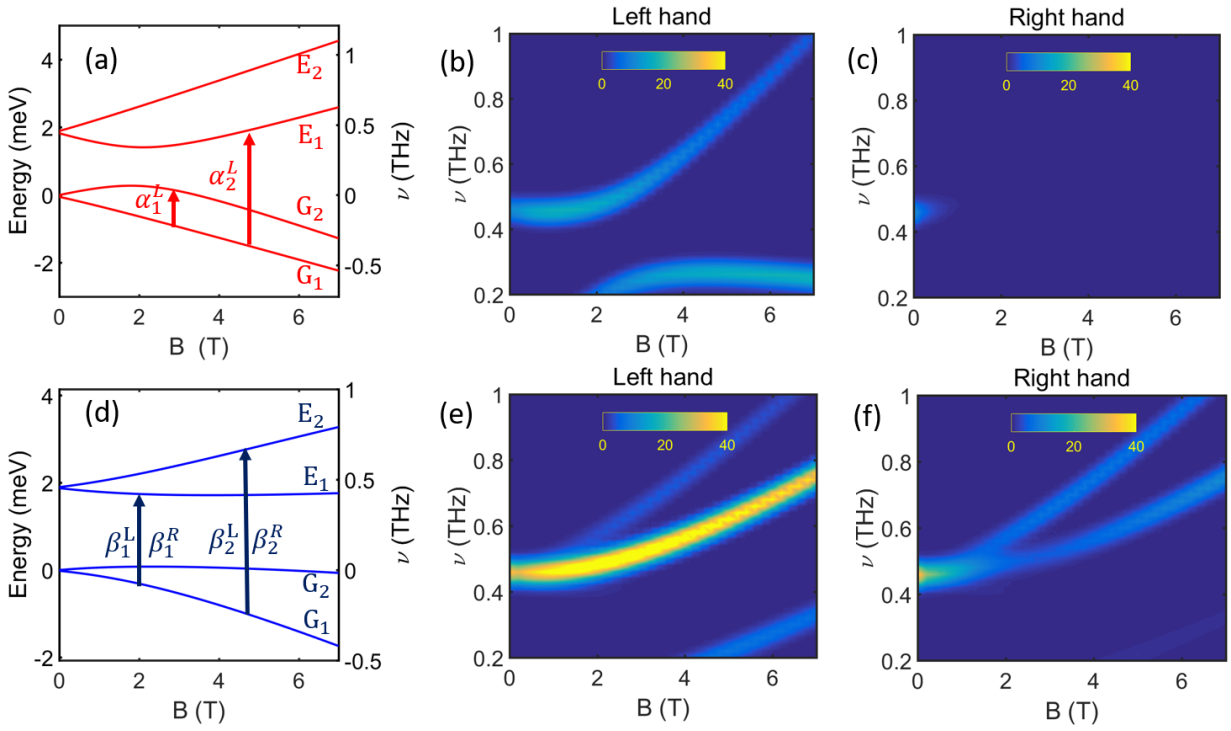


FIG. 2. **(a)** Calculated energy of four lowest crystal field as a function of field for Tb_α. The observed excitations α_1^L and α_2^L correspond to transition $G_1 \to G_2$ and $G_1 \to E_1$ of Tb_α. Colour plot of calculated intensity as function of energy and field for Tb_α in left **(b)** and right **(c)** channel. The weak intensity at low field in **(c)** is transition from thermally populated $G_2 \to E_2$. **(d)** Calculated energy of four lowest crystal field as a function of field for Tb_β. The observed excitations β_1^L,β_1^R and β_2^L,β_2^R correspond to transition $G_1 \to E_1$ and $G_1 \to E_2$ of Tb_β, respectively. **(e-f)** Colour plot of calculated intensity as function of energy and field for Tb_β in left and right.

Zeeman term

$$H_{Zeeman} = -\mu_B g_J \vec{B} \cdot \vec{J}. \quad (2)$$

By diagonalizing the Hamiltonian, we obtain the eigenenergies and eigenfunctions at each magnetic field. We calculate the spectra for Tb_α and Tb_β separately because the Zeeman term is different due to relative orientation of field with respect to the local [111] axis.

We plot the field evolution of the four lowest energy levels for Tb_α and Tb_β as shown in Fig. 2(a) and Fig. 2(d), respectively. The transitions between different states correspond closely to experimentally observed excitations. The CEF excitations couple to the magnetic field of the THz pulse. The general selection rule for magnetic dipole excitations is $\Delta m = 0, \pm 1$ and $\Delta J = 0, \pm 1$ with no parity change, which is already satisfied by the E_g symmetry of ground and first excited doublets. In the Faraday geometry with J=6 for Tb^{3+}, because of the conservation of angular momentum, excitations with $\Delta m = +1, -1$ should be seen in left and right channels, respectively. $\Delta m = 0$ is forbidden in the Faraday geometry. Based on selection rules, the transition $G_1 \to G_2$ and $G_1 \to E_1$ for Tb_α have $\Delta m = +1$ and should only be seen in the left channel as α_1^L and α_2^L. $G_1 \to E_2$ which would only be allowed with $\Delta m = 0$ cannot be seen in either left or right channels for Tb_α. Fig. 2(b) and (c) are color plots of computed spectra as function of magnetic field for Tb_α. The intensity is calculated based on Fermi's golden rule [49]. For Tb_β where the field is not along the local [111] direction and transverse components of the field makes the wavefunction a mix of $|\pm 4\rangle$ and $|\pm 5\rangle$, transitions at the β sites composed of $\Delta m = \pm 1$ can be seen in both left and right channel as shown in Fig. 2(e) and (f). For Tb_β, $G_1 \to E_1$ are observed as β_1^L and β_1^R in left and right channel with similar energies but different intensities. $G_1 \to E_2$ are observed as β_2^L and β_2^R as shown in Fig. 1(a) and (b).

The number of observed transitions, their intensities, their rough field dependence and even aspects of the anomalies are reproduced in the simple single ion model. One distinct feature is the kink-like behavior of α_2^L around 3 T, which might be taken to be indicative of a phase transition. In fact, Ref. [40] proposed a structural phase transition in a 2.3 T [111] field due to displacement of O″ to explain nonlinear phonon splitting under magnetic fields. Here we have shown this behavior can be understood from energy hybridization within the four lowest crystal energy levels, e.g., Fig. 2(a) shows level re-

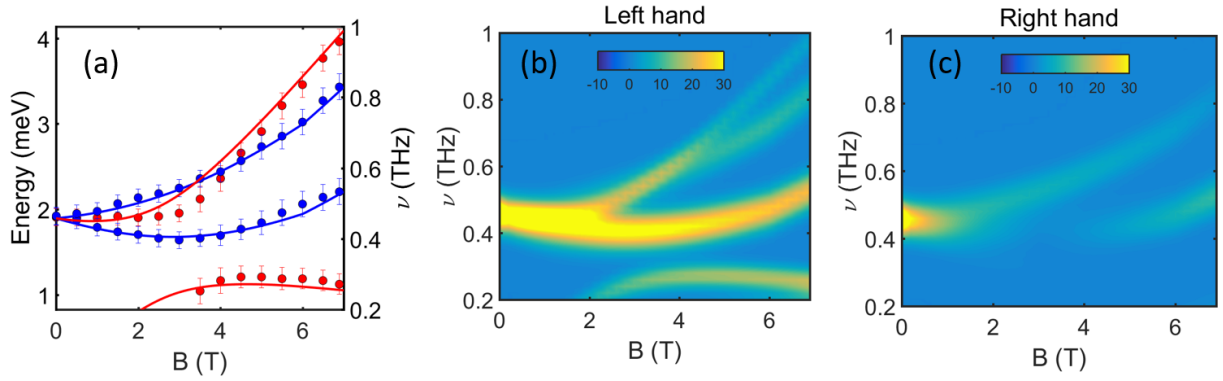


FIG. 3. **(a)** Comparison between experiment and calculated energy with consideration of field induced crystal field environment change. Red and blue represent Tb_α and Tb_β. Colour plot of calculated intensity as function of energy and field for Tb_α and Tb_β in left **(b)** and right **(c)** channel.

pulsion between G_2 and E_1 for Tb_α , which cause a sharp up-turn of α_2^L at 3 T as shown in Fig. 2(b). With increasing magnetic field, the intensity of α_1^L increases due to an enhanced transition amplitude based on Fermi's golden rule, which looks like a "new" excitation just appearing at 3 T. Therefore, we believe those sharp features come from low energy CEF hybridization instead of structural phase transition.

In the above calculation, with only single ion CEF and Zeeman terms involved, one can already explain the experiment reasonably well, but there remains some quantitative inconsistencies, particularly for the Tb_β contribution. For Tb_β, the transition $G_1 \rightarrow G_2$ should be visible in THz range but we do not observe it. In addition, both of the calculated transitions $G_1 \rightarrow E_1$ and $G_1 \rightarrow E_2$ are predicted to be much higher than the experimental data [49]. The discrepancies between experiments and calculations are more clear in phase sensitive techniques than with other optical methods [42]. Clearly, there are higher order effects we have not considered. We believe that magnetoelastic coupling or exchange interactions are not large effects in contrast to the conclusions in [42]. Although we find indirect evidence for magnetoelastic coupling, a small energy shift for the transition from the ground doublet G to first excited doublet E, the magnetoelastic coupling constant is limited by such small energy scale and has little contribution to the calculation [49]. Of course an exchange interaction is necessary to reproduce the dispersion of the CEFs, but it does not improve agreement as function of field at the Γ point [49]. Both moderate magnetoelastic couplings and exchange interactions can lead to finite splitting of the zero field doublets, which is inconsistent with an almost invisible splitting in the experiment. This gives an upper bound on their significance.

The preceding analysis treats the CEF Hamiltonian as independent of external magnetic field. However, the magnetic field can influence the crystal field environment as follows. The orbital angular momentum results from the spatially anisotropic $4f$ wave functions that can be envisioned as oblate electron charge cloud. Applying magnetic field along [111] direction aligns the spin of Tb and also the electron cloud because of spin-orbital coupling. This modifies the interaction between valence electrons of Tb and its neighbour ligands (O'') via Coulomb repulsion, which results in field induced crystal environment changes. This should be a ubiquitous effect although the influence is generally negligible. Here, such effect may be amplified due to the dynamic vibration of atoms, which makes the overlap between electrons clouds possibly larger. Therefore we incorporate magnetic field induced crystal field changes in our calculations. Applying a field reduces the symmetry for Tb_β from D_{3d} to C_1, which allows additional Stevens operators to appear in H_{CEF}. On the other hand, Tb_α remains D_{3d}, so we keep the same Stevens operators but adding extra field dependence to the original B_q^k. For simplicity, we approximate the dependence of the changes of CEF parameters to be linear on applied field. We fit the energy excitations to the refined model. As shown in Fig. 3(a), the experimental spectra can be reproduced essentially perfectly: the calculated energies of β_1 and β_2 for Tb_β are lower and match with data now; the transition $G_1 \rightarrow G_2$ is suppressed to below the THz range. The obtained ΔB_q^k is relatively small compared to the original B_q^k and has negligible impact on the high energy excitations. The good agreement between transmission amplitude Fig. 1 and the simulated intensity plots can be seen in Fig. 3 (b-c) for both left and right channels.

There are a few things to note. (1) For better agreement with experiment, we use a slightly reduced g factor $\sim$1.3 for the calculation instead of the Landé $g_J = 1.5$. This small correction only modifies the results slightly and does not change the essential features. There are

at least two possibilities for the reduced g factor. First, the Landé result assumes the LS coupling scheme (J=6) and ignores higher-order couplings that can reduce g. Moreover, the possibility of a dynamic Jahn-Teller effect has been reported [38, 50] that can lead to a reduced g factor due to quenching of the orbital moment [51]. (2) The coupling between magnetic field and the CEF changes the electron charge cloud and reduces the symmetry of Tb_β to C_1. This may lead to a displacement of atoms, e.g., O″, but not necessarily. With the likely dynamic Jahn-Teller effect in $Tb_2Ti_2O_7$, atoms may vibrate around the original position without having finite displacement [38, 50]. (3) The lower energies of Tb_β (with a reduced Zeeman splitting) can be phenomenologically understood as an induced internal magnetic field compensating the external field. With applied magnetic field, there is more overlap between the Tb and O electron cloud, which impedes the further rotation of the Tb electron clouds as well as spins due to spin-orbit coupling. This is equivalent to having an opposite internal field that compensates the external field, hence, suppressing the rotation of spins toward the [111] direction. With increasing the external field further, the spin of Tb_β gradually aligns with the magnetic field, and so during the fitting we have a threshold of magnetic field ~ 6 T, above which the ΔB_q^k does not change further.

In conclusion, we performed THz spectroscopy on high quality single crystal $Tb_2Ti_2O_7$ with a [111] magnetic field to study its low energy crystal field excitations. Anomalous crystal field excitations are observed and explained by low energy CEF hybridization. Single ion calculation with inclusion of the field induced changes to the crystal field environment is able to reproduce the spectra quantitatively. Our work suggests the interplay among multiple degrees of freedom in $Tb_2Ti_2O_7$ and sets a benchmark for calculating the crystal field excitations of spin liquid in magnetic field. In future experiments, ultrasonic measurements that are sensitive to elastic constant and diffraction measurements that can detect the displacement of O″ are desired. The exotic and diverse physics in $Tb_2Ti_2O_7$ deserves further experimental and theoretical investigations.

The authors would like to thank C. Broholm for helpful discussions and T. Fennell for helpful correspondence. This work at JHU was supported as part of the Institute for Quantum Matter, an EFRC funded by the DOE-BES under DE-SC0019331.

[1] L. Balents, Nature (London) **464**, 199 (2010).
[2] J. S. Gardner, M. J. P. Gingras, and J. E. Greedan, Rev. Mod. Phys. **82**, 53 (2010).
[3] A. P. Ramirez, A. Hayashi, R. J. Cava, R. Siddharthan, and B. Shastry, Nature **399**, 333 (1999).
[4] T. Fennell, P. Deen, A. Wildes, K. Schmalzl, D. Prabhakaran, A. Boothroyd, R. Aldus, D. McMorrow, and S. Bramwell, Science **326**, 415 (2009).
[5] S. T. Bramwell and M. J. Gingras, Science **294**, 1495 (2001).
[6] C. Castelnovo, R. Moessner, and S. L. Sondhi, Nature **451**, 42 (2008).
[7] D. J. P. Morris, D. Tennant, S. Grigera, B. Klemke, C. Castelnovo, R. Moessner, C. Czternasty, M. Meissner, K. Rule, J.-U. Hoffmann, *et al.*, Science **326**, 411 (2009).
[8] Y. Zhou, K. Kanoda, and T.-K. Ng, Rev. Mod. Phys. **89**, 025003 (2017).
[9] L. Savary and L. Balents, Reports on Progress in Physics **80**, 016502 (2016).
[10] A. Banerjee, C. Bridges, J.-Q. Yan, A. Aczel, L. Li, M. Stone, G. Granroth, M. Lumsden, Y. Yiu, J. Knolle, *et al.*, Nature materials **15**, 733 (2016).
[11] A. Y. Kitaev, Annals of Physics **303**, 2 (2003).
[12] J. A. Paddison, M. Daum, Z. Dun, G. Ehlers, Y. Liu, M. B. Stone, H. Zhou, and M. Mourigal, Nature Physics **13**, 117 (2017).
[13] T.-H. Han, J. S. Helton, S. Chu, D. G. Nocera, J. A. Rodriguez-Rivera, C. Broholm, and Y. S. Lee, Nature **492**, 406 (2012).
[14] A. Scheie, J. Kindervater, S. Zhang, H. Changlani, G. Sala, G. Ehlers, A. Heinemann, G. Tucker, S. Koohpayeh, and C. Broholm, arXiv preprint arXiv:1912.04913 (2019).
[15] K. A. Ross, L. Savary, B. D. Gaulin, and L. Balents, Physical Review X **1**, 021002 (2011).
[16] A. Scheie, J. Kindervater, S. Säubert, C. Duvinage, C. Pfleiderer, H. J. Changlani, S. Zhang, L. Harriger, K. Arpino, S. M. Koohpayeh, O. Tchernyshyov, and C. Broholm, Phys. Rev. Lett. **119**, 127201 (2017).
[17] L. Pan, N. Laurita, K. A. Ross, B. D. Gaulin, and N. Armitage, Nature Physics **12**, 361 (2016).
[18] L. D. C. Jaubert, O. Benton, J. G. Rau, J. Oitmaa, R. R. P. Singh, N. Shannon, and M. J. P. Gingras, Phys. Rev. Lett. **115**, 267208 (2015).
[19] J. Robert, E. Lhotel, G. Remenyi, S. Sahling, I. Mirebeau, C. Decorse, B. Canals, and S. Petit, Phys. Rev. B **92**, 064425 (2015).
[20] J. S. Gardner, S. R. Dunsiger, B. D. Gaulin, M. J. P. Gingras, J. E. Greedan, R. F. Kiefl, M. D. Lumsden, W. A. MacFarlane, N. P. Raju, J. E. Sonier, I. Swainson, and Z. Tun, Phys. Rev. Lett. **82**, 1012 (1999).
[21] K. Arpino, B. Trump, A. Scheie, T. McQueen, and S. Koohpayeh, Physical Review B **95**, 094407 (2017).
[22] M. J. P. Gingras, B. C. den Hertog, M. Faucher, J. S. Gardner, S. R. Dunsiger, L. J. Chang, B. D. Gaulin, N. P. Raju, and J. E. Greedan, Phys. Rev. B **62**, 6496 (2000).
[23] T. Fennell, M. Kenzelmann, B. Roessli, M. K. Haas, and R. J. Cava, Phys. Rev. Lett. **109**, 017201 (2012).
[24] M. Ruminy, E. Pomjakushina, K. Iida, K. Kamazawa, D. T. Adroja, U. Stuhr, and T. Fennell, Phys. Rev. B **94**, 024430 (2016).
[25] J. Zhang, K. Fritsch, Z. Hao, B. V. Bagheri, M. J. P. Gingras, G. E. Granroth, P. Jiramongkolchai, R. J. Cava, and B. D. Gaulin, Phys. Rev. B **89**, 134410 (2014).
[26] A. J. Princep, H. C. Walker, D. T. Adroja, D. Prabhakaran, and A. T. Boothroyd, Phys. Rev. B **91**, 224430 (2015).
[27] T. T. A. Lummen, I. P. Handayani, M. C. Donker, D. Fausti, G. Dhalenne, P. Berthet, A. Revcolevschi, and

P. H. M. van Loosdrecht, Phys. Rev. B **77**, 214310 (2008).
[28] H. R. Molavian, M. J. P. Gingras, and B. Canals, Phys. Rev. Lett. **98**, 157204 (2007).
[29] C. Liu, F.-Y. Li, and G. Chen, Phys. Rev. B **99**, 224407 (2019).
[30] B. D. Gaulin, J. S. Gardner, P. A. McClarty, and M. J. P. Gingras, Phys. Rev. B **84**, 140402 (2011).
[31] P. Bonville, I. Mirebeau, A. Gukasov, S. Petit, and J. Robert, Phys. Rev. B **84**, 184409 (2011).
[32] S. H. Curnoe, Phys. Rev. B **78**, 094418 (2008).
[33] K. Rule and P. Bonville, in *Journal of Physics: Conference Series*, Vol. 145 (IOP Publishing, 2009) p. 012027.
[34] V. Klekovkina and B. Malkin, Optics and Spectroscopy **116**, 849 (2014).
[35] T. Fennell, M. Kenzelmann, B. Roessli, H. Mutka, J. Ollivier, M. Ruminy, U. Stuhr, O. Zaharko, L. Bovo, A. Cervellino, *et al.*, Physical review letters **112**, 017203 (2014).
[36] E. Constable, R. Ballou, J. Robert, C. Decorse, J.-B. Brubach, P. Roy, E. Lhotel, L. Del-Rey, V. Simonet, S. Petit, *et al.*, Physical Review B **95**, 020415 (2017).
[37] M. Ruminy, S. Guitteny, J. Robert, L.-P. Regnault, M. Boehm, P. Steffens, H. Mutka, J. Ollivier, U. Stuhr, J. S. White, B. Roessli, L. Bovo, C. Decorse, M. K. Haas, R. J. Cava, I. Mirebeau, M. Kenzelmann, S. Petit, and T. Fennell, Phys. Rev. B **99**, 224431 (2019).
[38] J. P. C. Ruff, B. D. Gaulin, J. P. Castellan, K. C. Rule, J. P. Clancy, J. Rodriguez, and H. A. Dabkowska, Phys. Rev. Lett. **99**, 237202 (2007).
[39] J. P. C. Ruff, Z. Islam, J. P. Clancy, K. A. Ross, H. Nojiri, Y. H. Matsuda, H. A. Dabkowska, A. D. Dabkowski, and B. D. Gaulin, Phys. Rev. Lett. **105**, 077203 (2010).
[40] F. Jin, C. Liu, Y. Chang, A. Zhang, Y. Wang, W. Liu, X. Wang, Y. Sun, G. Chen, X. Sun, and Q. Zhang, Phys. Rev. Lett. **124**, 087601 (2020).
[41] C. Morris, R. V. Aguilar, A. Ghosh, S. Koohpayeh, J. Krizan, R. Cava, O. Tchernyshyov, T. McQueen, and N. Armitage, Physical review letters **112**, 137403 (2014).
[42] K. Amelin, Y. Alexanian, U. Nagel, T. Rõ om, J. Robert, J. Debray, V. Simonet, C. Decorse, Z. Wang, R. Ballou, E. Constable, and S. de Brion, Phys. Rev. B **102**, 134428 (2020).
[43] X. Zhang, F. Mahmood, M. Daum, Z. Dun, J. A. M. Paddison, N. J. Laurita, T. Hong, H. Zhou, N. P. Armitage, and M. Mourigal, Phys. Rev. X **8**, 031001 (2018).
[44] L. Pan, S. K. Kim, A. Ghosh, C. M. Morris, K. A. Ross, E. Kermarrec, B. D. Gaulin, S. Koohpayeh, O. Tchernyshyov, and N. Armitage, Nature communications **5**, 4970 (2014).
[45] N. P. Armitage, Phys. Rev. B **90**, 035135 (2014).
[46] C. M. Morris, R. V. Aguilar, A. V. Stier, and N. P. Armitage, Optics Express **20**, 12303 (2012).
[47] N. Laurita, J. Deisenhofer, L. Pan, C. Morris, M. Schmidt, M. Johnsson, V. Tsurkan, A. Loidl, and N. Armitage, Physical review letters **114**, 207201 (2015).
[48] M. Hutchings, in *Solid State Physics* (Elsevier, 1964) pp. 227–273.
[49] See Supplemental Material at [] for the description of the setup and details of the crystal field calculationseffects of the exchange interactions and magnetoelastic coupling..
[50] P. Bonville, A. Gukasov, I. Mirebeau, and S. Petit, Phys. Rev. B **89**, 085115 (2014).
[51] F. S. Ham, Phys. Rev. **138**, A1727 (1965).